Research Article | Vol. 12, No. 9 / 1 Sep 2022 / Optical Materials Express 3621
Optical Materials EXPRESS

Impact of rare earth doping on the luminescence of lanthanum aluminum silicate glasses for radiation sensing

Ruth E. Shaw,[1] Christopher A. G. Kalnins,[1] Carly A. Whittaker,[1,2] Jillian E. Moffatt,[1] Georgios Tsiminis,[1] Elizaveta Klantsataya,[1] David Ottaway,[1] Nigel A. Spooner,[1,3] Doris Litzkendorf,[4] Anne Matthes,[4] Anka Schwuchow,[4] Katrin Wondraczek,[4] and Heike Ebendorff-Heidepriem[1,*]

[1]*Institute for Photonics and Advanced Sensing and School of Physical Sciences and Australian Research Council Australian Copper-Uranium Transformation Research Hub, University of Adelaide, Adelaide, 5005, Australia*
[2]*GenesisCare Adelaide, Adelaide, 5000, Australia*
[3]*Defence Science & Technology Group, Edinburgh 5111, SA, Australia*
[4]*Leibniz Institute of Photonic Technology, Competence Center for Specialty Optical Fibers and Fiber Research and Technology, Albert-Einstein-Str. 9, Jena, 07745, Germany*
[*]*heike.ebendorff@adelaide.edu.au*

Abstract: Large core soft glass fibers have been demonstrated to be promising candidates as intrinsic fiber sensors for radiation detection and dosimetry applications. Doping with rare earth ions enhanced their radiation sensitivity. SiO_2-Al_2O_3-La_2O_3 (SAL) glasses offer easy fabrication of large core fibers with high rare earth concentration and higher mechanical strength than soft glasses. This paper evaluates the suitability of the SAL glass type for radiation dosimetry based on optically stimulated luminescence (OSL) via a comprehensive investigation of the spectroscopic and dosimetric properties of undoped and differently rare earth doped bulk SAL glass samples. Due to the low intensity of the rare earth luminescence peaks in the 250–400 nm OSL detection range, the OSL response for all the SAL glasses is not caused by the rare earth ions but by radiation-induced defects that act as intrinsic centers for the recombination of electrons and holes produced by the ionizing radiation, trapped in fabrication induced defect centers, and then released via stimulation with 470 nm light. The rare earth ions interfere with these processes involving intrinsic centers. This dosimetric behavior of highly rare earth doped SAL glasses suggests that enhancement of OSL response requires lower rare earth concentrations and/or longer wavelength OSL detection range.

1. Introduction

Optical fibers that are sensitive to ionizing radiation have been demonstrated to be a viable tool for radiation portal sensors, monitoring naturally occurring radiation, such as during mineral processing, and radiation dosimeters because they allow real-time, continuous monitoring in hard to access areas [1–3] in a low-cost and low-power form. The mechanism of radiation-induced attenuation is generally used to measure radiation flux for higher radioactivity doses such as for monitoring nuclear facilities [4,5]. Most optical fiber dosimetry research has been based on scintillation (radioluminescence (RL)) [3,6–9], with prompt radiation response during radiation exposure [10]. Measurement of accumulated radiation dose requires the use of thermally (TL) or optically stimulated luminescence (OSL) as sensing method after the radiation exposure [11]. However, TL is impractical for fiber applications, and there are only limited studies on the use of

#463119 https://doi.org/10.1364/OME.463119
Journal © 2022 Received 6 May 2022; revised 10 Jul 2022; accepted 11 Jul 2022; published 15 Aug 2022

Optical Materials EXPRESS

OSL for intrinsic fiber dosimetry [3,12–14]. A recent example is the demonstration of radiation detection via OSL for fluoride-phosphate soft glass fibers [12]. The addition of rare earth dopants was shown to enhance sensitivity of luminescence-based detection techniques such as TL, RL and OSL [15–18].

The study of fluoride-phosphate glass fibers has shown that single material large core fibers (also referred to as core-only or air-clad fibers) are ideally suited as intrinsic fiber dosimeters, whereby the whole fiber core along the whole fiber length is sensitive to ionizing radiation. These fibers demonstrate intense OSL response since the whole fiber represents the sensing region, leading to enhanced detection surface area and volume [12,15].

Compared to soft glasses such as fluoride-phosphate glass, silica based fibers offer a more physically robust and optically efficient alternative due to the high intrinsic mechanical strength [19], thermal resistance [20] and low optical loss [21] of silica. Short length of copper doped silica rod attached to the tip of a conventional silica optical fiber was tested for OSL. However, due to its extrinsic sensing functionality, where the optical fiber is only used to guide the light to and from the sensing region, this fiber dosimeter approach is restricted to measuring single point locations [1,22]. Furthermore, the sensitivity of such sensors is limited due to small detection surface area and volume. By contrast, silica made using the reactive powder sintering technique (REPUSIL) [23] allows for the fabrication of large core silica fibers with homogeneous rare earth doping in the core, providing intrinsic sensing functionality and large detection volume. To date, the study of the dosimetry properties of rare earth doped REPUSIL silica in form of bulk glass samples with low doping levels yielded promising results [18].

While the rare earth doping concentration for REPUSIL derived silica is limited to about 0.6 mol% rare earth oxide [24] by the amount of co-dopant Al_2O_3 that can be incorporated with this technique, which efficiently prevents rare earth clustering [25,26], lanthanum aluminum silicate glasses (SiO_2-Al_2O_3-La_2O_3 (SAL)) can be doped with one order of magnitude higher rare earth concentration of up to 6 mol% rare earth oxide due to different glass composition (high concentrations of Al_2O_3 and La_2O_3) and different glass fabrication method (melt-quench technique). This makes SAL glasses well suited for the fabrication of large core fibers with high and homogeneous rare earth doping over the whole fiber core volume [24,27] for intrinsic fiber dosimetry.

In this paper, we investigate the spectroscopic and dosimetric properties of bulk SAL glass samples without dopants and with high concentrations of the luminescent rare earth (RE) ions (Ce^{3+}, Tb^{3+}, Ho^{3+}, Tm^{3+}) to evaluate the potential of rare earth doping on OSL-based dosimetry of SAL glass, which is a promising glass type for large core fiber fabrication. In the first part of the paper, absorbance and photoluminescence (PL) spectroscopy is used to reveal the presence of absorption and luminescence transitions within the bandgap of the glass matrix before exposure to ionizing radiation. RL and TL spectroscopy reveals all luminescence transitions stimulated during and after radiation exposure. Comparison to PL (before radiation exposure) is used to reveal which luminescent transitions can act as recombination centers and thus might cause OSL. TL spectroscopy also shows the thermal stability (and hence long-term room temperature stability) of radiation-induced traps and recombination centers, which helps to understand OSL response behavior for dosimetry. In the second part of the paper, the OSL response behavior is studied comprehensively in terms of decay behavior, integrated counts, pulse-annealing, repeated and delayed measurements and phosphorescence measurement to evaluate suitability for various dosimetric applications. To understand the impact of high RE concentration in SAL glasses, the spectroscopic and dosimetric properties of the Ce^{3+} and Tm^{3+} doped SAL glass samples are compared with Ce^{3+} and Tm^{3+} doped REPUSIL silica samples with 100 times lower RE concentration and also in bulk glass geometry. To understand the impact of the glass matrix itself, the OSL response of undoped SAL glass is compared with undoped REPUSIL glass. The investigation of the spectroscopic and dosimetric properties show that the RE features

Optical Materials EXPRESS

(concentration, luminescent transition type, luminescence wavelength relative to OSL detection range and absorption at the stimulation wavelength) have a pronounced impact on OSL behavior while both the undoped SAL and REPUSIL glasses exhibit similar OSL behavior.

2. Sample compositions and experimental methods

The SAL glasses were prepared using a crucible melt quenching technology [24,27]. High-purity SiO_2, La_2O_3, Ho_2O_3, Tm_2O_3, Tb_2O_3, Yb_2O_3, Ce_2O_3 and $Al(OH)_3$ raw materials were melted at 1400–1650 °C and then fritted in ultra-pure water. The dried glass frit was remelted at 1,650 °C and then poured into stainless steel molds to form homogeneous, bubble-free blocks. The cast glass blocks were annealed around the glass transition temperature and then slowly cooled to room temperature. The composition of the fabricated glasses was determined by quantitative Electron Probe Micro Analysis (EPMA) using Wavelength Dispersive X-ray analysis (WDX, JEOL JXA-8800L). The Ce^{3+} and Tm^{3+} doped REPUSIL silica samples reported in [18] are included for comparison with the Ce^{3+} and Tm^{3+} doped SAL glass samples. The fabrication procedure and composition analysis of these samples is described in [18]. Furthermore, undoped REPUSIL glass without any RE and other dopants is investigated. The RE ion concentrations were calculated from the measured composition and the glass density. For the SAL samples, the SAL glass density of 3.3 g/cm^3 from Ref. [28] was used. For the REPUSIL samples, the silica density of 2.2 g/cm^3 from Ref. [29] was used. Table 1 lists the sample names (based on RE ion concentration), nominal batch and measured glass compositions, and RE concentrations of the samples investigated. The deviation of the measured compositions from the nominal compositions is less than 10%. To reflect the two orders of magnitude difference in RE concentration for the two glass types, the terminology of weakly doped REPUSIL glasses and highly doped SAL glasses is used.

Table 1. Compositions of the SAL and REPUSIL samples. The values in parentheses indicate the nominal composition according to the glass batch, the other values indicate the composition of the fabricated samples measured using EPMA. The RE ion concentration is based on the measured glass composition.

sample name	RE ion	(nominal) measured composition (mol%)				RE ion concentration (10^{20} ions/cm^3)
		SiO_2	Al_2O_3	La_2O_3	RE_2O_3	
undoped SAL	none	(70) 70.00	(20) 18.76	(10) 11.24		0
0.42 Ho SAL	Ho^{3+}	(70) 71.06	(20) 18.94	(9.9) 9.90	(0.1) 0.10	0.42
1.13 Ho SAL	Ho^{3+}	(70) 71.12	(20) 18.79	(9.7) 9.82	(0.3) 0.27	1.13
2.24 Tm SAL	Tm^{3+}	(70) 69.42	(20) 20.40	(9.4) 9.64	(0.6) 0.54	2.24
3.45 Tm SAL	Tm^{3+}	(70) 69.31	(20) 20.73	(9.125) 9.13	(0.875) 0.83	3.45
4.33 Tb SAL	Tb^{3+}	(70) 64.38	(20) 24.82	(9.125) 9.76	(0.875) 1.04	4.33
1.25 Ce SAL	Ce^{3+}	(70) 71.50	(20) 19.70	(9.5) 8.50	(0.5) 0.3	1.25
undoped REPUSIL	none	(100)				0
0.02 Tm REPUSIL	Tm^{3+}	(99.9) 99.41	(0.1) 0.58	(0.0) 0.000	(0.005) 0.005	0.02
0.02 Ce REPUSIL	Ce^{3+}	(99.9) 99.77	(0.1) 0.22	(0.0) 0.001	(0.005) 0.005	0.02

For measurement of the absorbance, PL and RL spectra, slides were cut from each sample and polished to 1 mm thickness. For measurement of the TL spectra and OSL counts, materials were crushed to grain sizes of 125–300 µm [30,31]. All experiments were performed with the same equipment and same experimental set up as used for REPUSIL samples previously [18], to allow a direct comparison of the SAL glass samples with selected REPUSIL glass samples investigated previously [18]. The experiments and details of the experimental conditions are listed in Table S1.

Optical Materials EXPRESS

The absorbance spectra were measured with a commercial UV-VIS-NIR spectrophotometer from Varian using a zero base line correction. Note that the step-feature at 800 nm for the absorbance spectra is an artefact caused by a detector change.

The PL spectra were measured using for excitation a 7 ns pulsed, 9 mm beam diameter tuneable laser (Opotek Radiant 355 with UV option; OPOTEK Inc, Carlsbad, CA) and for detection a Princeton Instruments Acton CCD array (SpectraPro 2300; Roper Scientific, Trenton, NJ) with Lightfield Software (Princeton Instruments, Trenton, NJ). Excitation was provided at 240, 280, 320, 340, 360, and 400 nm with directly scattered light removed using a 355 nm long pass filter (BLP01-355R-25, Semrock, USA) for the Ce doped samples and a 430 nm long pass filter (FF01-430/LP, Semrock, USA) for all other samples. The background spectra were also measured and subtracted. The spectra were normalized for excitation pulse power at each excitation wavelength.

Ionizing radiation exposures were performed using solid-state foils (Amersham International, UK) ^{90}Sr/^{90}Y source for beta irradiation. The RL spectra were measured with a Princeton Instruments Spectrofluorimeter incorporating an Acton "SpectraPro 2300i" double monochromator and a PIXIS 256 TE-cooled spectrographic CCD. The TL emission spectra were measured using an in-house custom built "3D-TL Spectrometer", incorporating a Littlemore TL Glow Oven interfaced to a modified Michelson interferometer [31]. The OSL was measured using a Risø TL/OSL DA-20 instrument incorporating a bi-alkai photomultiplier tube and an on-board calibrated Sr^{90}/Y^{90} 1.5 GBq beta source. For the RL measurements, background and cosmic ray events were subtracted, and the measured intensity was normalized for the activity of the beta particle source. The measured RL and TL spectra, as well as OSL and phosphorescence counts were normalized for mass and dose. For TL measurement, the samples were heated at a rate of 5 K/s. For OSL measurement, a Hoya U340 filter was used for detection in the 250–400 nm wavelength, and a 30 mW laser diode array with 7 mm diameter beam size was used for stimulation at 470 nm.

3. Results and discussion

3.1. Absorbance characteristics

The absorbance spectra are shown in Fig. 1. The undoped SAL and REPUSIL samples show no RE peaks, indicating absence of any RE contamination. The RE doped samples show the narrow peaks due to the respective f-f transitions of the RE ions [32] (Table S2). Increased Tm and Ho concentrations result in increased absorbance of the RE peaks (Fig. S1).

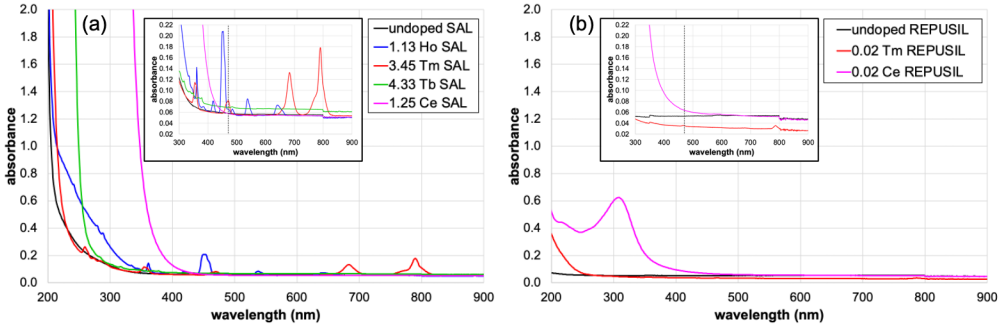

Fig. 1. Absorbance spectra of 1 mm thick polished slides of undoped and RE doped (a) SAL glass samples and (b) REPUSIL silica samples. The insets show the spectra with different absorbance scale. The dashed lines indicate the stimulation wavelength.

Optical Materials EXPRESS

Due to the high absorbance intensity of the spin-allowed f-d transition of the RE ions in the highly doped SAL samples, for the sample thickness of 1 mm used here, only the tail of the f-d absorption band is observed in the form of an UV edge. For the Ho doped SAL sample, the UV edge is at the same position as the undoped SAL samples, indicating that the high-intensity intrinsic glass absorbance in the UV at ~200 nm masks the f-d transition absorption tail. This is consistent with the significantly shorter f-d peak wavelength of Ho^{3+} at 156 nm in a fluoride crystal [33] compared to the UV edge at 210 nm in the undoped SAL sample. Note that higher absorbance of the Ho samples between 200 and 380 nm when compared to the undoped sample could potentially be due to iron (Fe^{3+}) impurities [34,35]. For the other RE doped SAL samples (Tm, Tb, Ce), the wavelength position of the UV edge is shifted to longer wavelengths compared to the undoped SAL sample due to longer peak wavelengths for the f-d transitions in these samples compared to the Ho sample. Specifically, the UV edge wavelength of the samples increases in the order of undoped (210 nm) = Ho (210 nm) ≤ Tm (220 nm) < Tb (250 nm) < Ce (330 nm) (Fig. 1(a)), which is in accordance with the f-d peak wavelengths of the RE ions in a fluoride crystal increasing in the order of Ho^{3+} (156 nm) < Tm^{3+} (164 nm) < Tb^{3+} (221 nm) < Ce^{3+} (312 nm) [33].

As expected for silica glass, the undoped REPUSIL sample shows only the low-intensity tail of the intrinsic glass edge within the measurement wavelength range of ≥200 nm. For the weakly doped REPUSIL samples, the main Ce^{3+} f-d band at 310 nm is clearly resolved, while for the Tm^{3+} f-d absorption only the tail of the band is within the measurement range in accordance with the shorter peak wavelength for Tm^{3+} compared to Ce^{3+}.

3.2. Photo-, radio- and thermo-luminescence (PL, RL and TL) characteristics

The PL spectra for excitation wavelengths yielding highest luminescence intensity are shown in Fig. 2, (other excitation wavelengths see Fig. S2). The RL and TL spectra are shown in Figs. 2 and 3. The peak wavelengths of the observed luminescence transitions are listed in Table S2. The luminescence spectra reveal three different types of transitions.

(a) Narrow luminescence bands from transitions between 4f levels for Tb^{3+} ions (low-intensity peaks at 380, 420 and 440 nm from the $^5D_3$ level; high-intensity peaks at 490, 540, 590 and 610 nm from the $^5D_4$ level to the various lower energy levels), and for Tm^{3+} ions (low-intensity peaks at 360 and 790 nm; high-intensity peak at 465 nm).

(b) A broad luminescence band at ~400 nm from the transition between the 5d and 4f levels of the Ce^{3+} ions.

(c) Broad low-intensity bands that do not coincide with any RE transitions and hence are attributed to intrinsic glass defect centers: at 520 nm and 740 nm in the undoped and Ho SAL samples, at 520 nm in the Tm SAL sample, and at 770 nm in the Ce SAL sample. In the Tb SAL, Tm REPUSIL and Ce REPUSIL samples, potential luminescence from intrinsic glass defects is masked by the intense RE luminescence. Note that no intrinsic glass defect luminescence is observed for RL and TL.

The presence of PL from intrinsic defect centers for SAL samples without exposure to beta radiation indicates the formation of these defects during SAL glass fabrication. The intrinsic glass defect with PL at 520 nm coincides with an intrinsic defect in silica, which shows PL at ~550 nm, whereby the atom structure of this defect is still under debate [36]. Despite extensive literature search, we could not find an intrinsic glass defect in oxide glasses, which shows PL at 740 nm. The absence of RL and TL from these defects suggests that they do not act as recombination centers, but they could act as traps within the OSL process.

Optical Materials EXPRESS

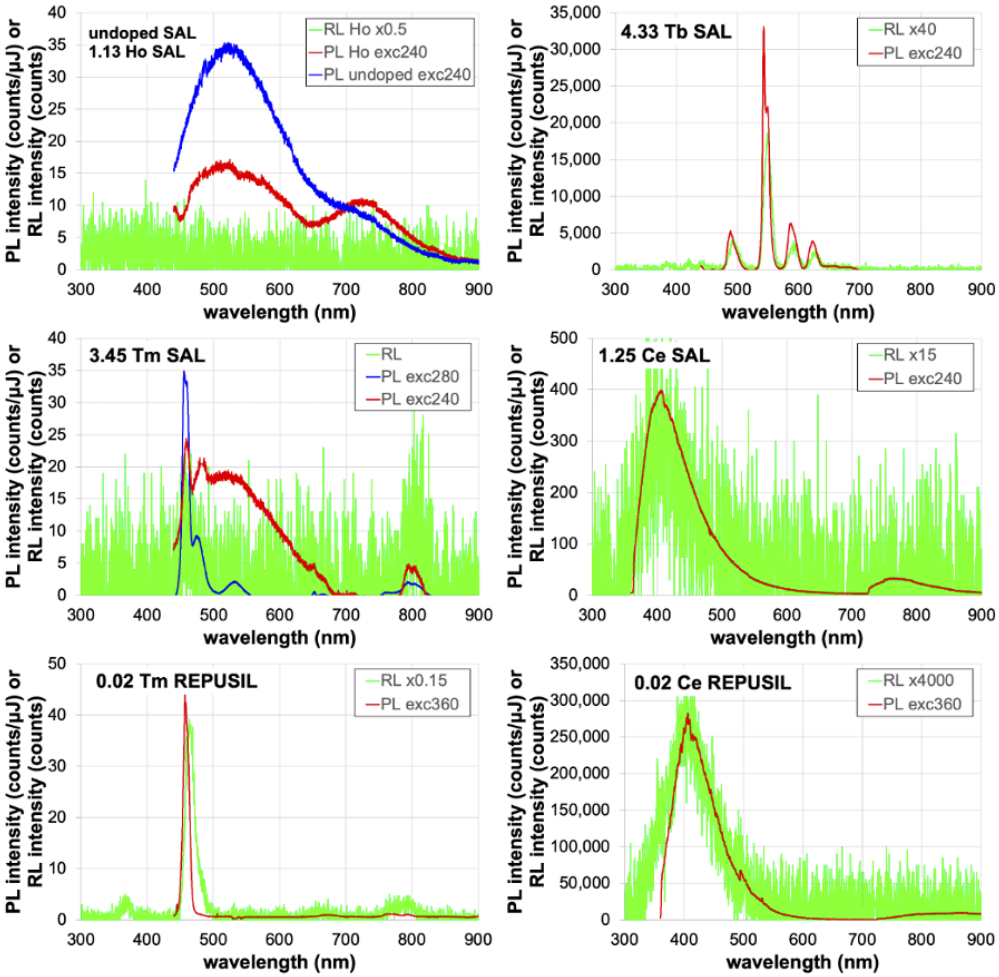

Fig. 2. PL spectra over an integration time of 5 seconds at an excitation wavelength yielding highest PL and RL spectra after 185 MBq beta radiation over an integration time of 10 seconds for SAL and REPUSIL samples. The RL spectra are scaled with the factors given in the legends.

Optical Materials EXPRESS

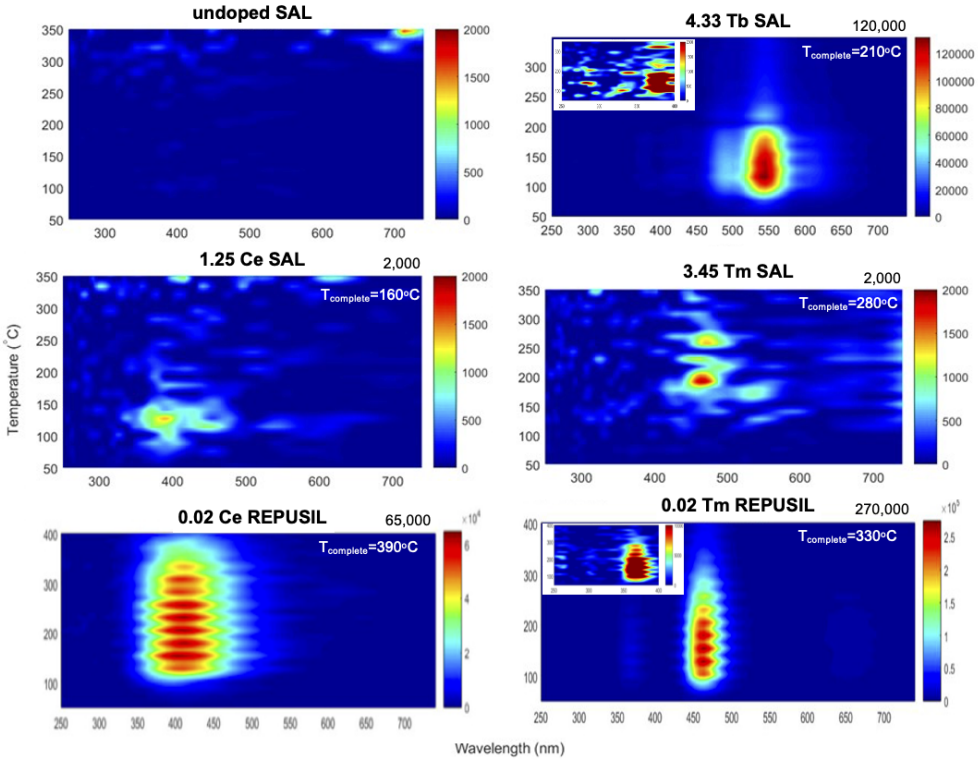

Fig. 3. TL spectra of SAL and REPUSIL glass samples after irradiation with a dose of 10 Gy. The numbers in black font at the top-right of each graph indicates the maximum TL intensity. The insets for the Tb SAL and Tm REPUSIL samples show the TL spectra at a scale of 0-2000 and 0-10000, respectively, for the wavelength range 250-400 nm.

The intensity of a specific RE luminescence peak depends on the position of the RE f-d absorption relative to the intrinsic glass edge, radiative transition probability, multiphonon decay, and RE concentration quenching as follows.

For Tm^{3+}, Tb^{3+} and Ce^{3+} in SAL and REPUSIL glasses, the RE f-d absorption is shifted to longer wavelengths away from the intrinsic glass edge, allowing efficient excitation of PL for these ions via f-d absorption.

The absence of any Ho^{3+} PL, RL and TL peaks in the SAL samples is attributed to quenching of the Ho^{3+} luminescence via non-radiative multiphonon decay. The rate of this process increases exponentially with decreasing energy gap between 4f energy levels and increasing phonon energy of the host glass [37]. For Ho^{3+}, all 4f energy levels in the UV-visible have small energy gaps ($<3000\ cm^{-1}$), yielding a multiphonon decay rate that is $\sim 20\times$ higher compared to Tb^{3+} and Tm^{3+}, which exhibit much larger energy gaps ($>6000\ cm^{-1}$) to the next lower energy level (Tb: $^5D_3$ 380 nm, $^5D_4$ 485 nm; Tm: $^1D_2$ 360 nm, $^1G_4$ 465 nm, $^3H_4$ 790 nm) and hence negligible multiphonon decay for transitions from these levels. Silicate glasses such as SAL have high phonon energy of $\sim 1100\ cm^{-1}$ [38], which leads to high multiphonon decay rate. Hence, Ho^{3+} PL was only observed for materials with low-phonon energy ($\leq 500\ cm^{-1}$) such as fluorides [39,40]. The effective multiphonon quenching of Ho^{3+} f-f luminescence due to small f-f energy gaps in the UV-visible and high phonon energy of the SAL glass cause the absence of any Ho^{3+} luminescence in SAL glass, and so the Ho sample behaves like the undoped sample.

Optical Materials EXPRESS

For the weakly doped Tm and Ce REPUSIL samples without concentration and multiphonon quenching due to low RE concentration and large energy gaps, respectively, the PL intensities of the Ce^{3+} peak at ~400 nm and the Tm^{3+} peaks at 360, 465, and 790 nm relative to each other are attributed to differences in the radiative transition probabilities of these transitions. The exceptionally high PL of Ce REPUSIL is due to high radiative transition probability of the spin-allowed d-f luminescence and effective excitation via f-d absorption. In contrast to PL, the RL and TL intensities of the main Tm^{3+} luminescence peak at 465 nm are larger than the RL and TL intensities of the Ce^{3+} luminescence peak at ~400 nm. A possible explanation is that high f-d absorption enhances PL but hampers RL and TL.

The two orders of magnitude larger RE concentrations of the highly doped SAL samples (2-4×10^{20} RE ions cm^{-3}) compared with the weakly doped REPUSIL samples (0.02×10^{20} RE ions cm^{-3}) has a significant effect on the intensity of the luminescence peaks. Figure 4(a) shows the decrease of the PL, RL and TL peak intensities with increased RE concentration for the Tm^{3+} f-f transition at 465 nm and the Ce^{3+} f-d transitions at 400 nm. Figure 4(b) demonstrates that the magnitude of the concentration quenching depends on the luminescence type.

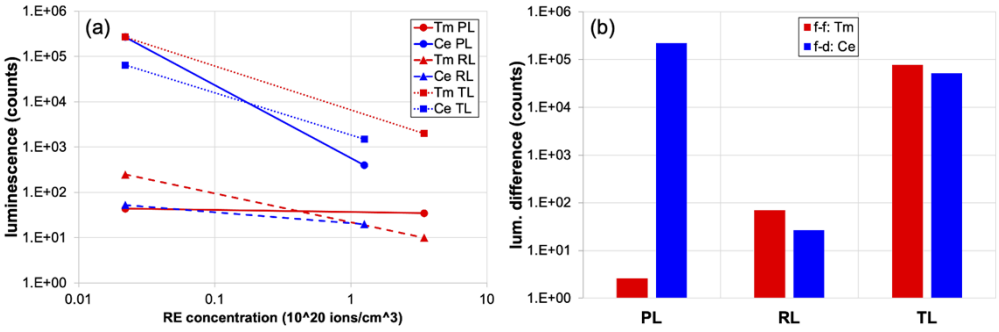

Fig. 4. (a) PL in counts/μJ and RL and TL in counts as a function of RE concentration for Tm REPUSIL, Tm SAL, Ce SAL and Ce REPUSIL samples. The lines are shown as guide for the eye. (b) Difference of luminescence (PL, RL, TL) between weakly and highly doped RE samples shown in (a).

PL shows negligible quenching for the f-f transitions and strong quenching for the f-d transitions. In contrast, RL and TL show similar concentration quenching behavior for both transitions. The former effect is attributed to the strong re-absorption of the PL due to the strong f-d absorption compared to the weak f-f absorption for the sample geometry used. The strong concentration quenching of both the d-f and f-f transitions for RL and TL suggests strong re-absorption effect for both RE transition types, possibly due to overall weak RL and TL intensity from RE ions relative to the absorption by the RE ions.

For the Tb^{3+} ions, the blue luminescence at 380 nm from the $^5D_3$ level is known to be quenched by cross relaxation, which depopulates the $^5D_3$ level to the $^5D_4$ level [41]. The enhanced population of the $^5D_4$ level increases the green luminescence at 540 nm from this level. As cross relaxation becomes more efficient with increasing Tb^{3+} concentration, the highly doped Tb SAL sample shows low-intensity blue PL, RL, and TL at 380 nm but high-intensity green PL, RL, and TL at 540 nm.

The TL spectra allow assessment of the lifetimes of the traps at ambient temperature. An increase in peak (untrapping) temperature typically reflects an increase in trap depth, hence also in the lifetime of the radiation-induced electron and hole defect centers at ambient temperature [11,42]. Considering the high-intensity TL peaks of the SAL samples (Tm - 465 nm, Tb - 540 nm, Ce - 400 nm), the lowest temperature for complete untrapping of the electrons (i.e. disappearance of TL) is approximately 280 °C for Tm, 210 °C for Tb and 160 °C for Ce doping (Fig. 3).

Optical Materials EXPRESS

Compared to the respective SAL samples, the REPUSIL samples require higher temperatures of 330 °C for Tm and 390 °C for Ce. This result suggests long-lived defects at room temperature in the REPUSIL samples. The difference in TL behavior for the RE doped SAL and REPUSIL samples correlates with their difference in composition, fabrication method and RE concentration as described in Section 2.

3.3. Optically stimulated luminescence (OSL) decay behavior

The OSL decay was measured as the time evolution of the luminescence counts promptly after beta irradiation in the 250-400 nm detection range under continuous stimulation at 470 nm wavelength for 1000 s. The OSL decay curves after 1 or 33 Gy dose are displayed in Fig. 5. The undoped as well as the Ho and Ce SAL and REPUSIL samples show the same OSL decay behavior; an initial high number of OSL counts followed by fast bleaching within ~200 s to a steady OSL level with negligible counts. The Tb SAL sample shows a similar behavior but with faster decay of ~20 s to a level with ~6x higher OSL counts.

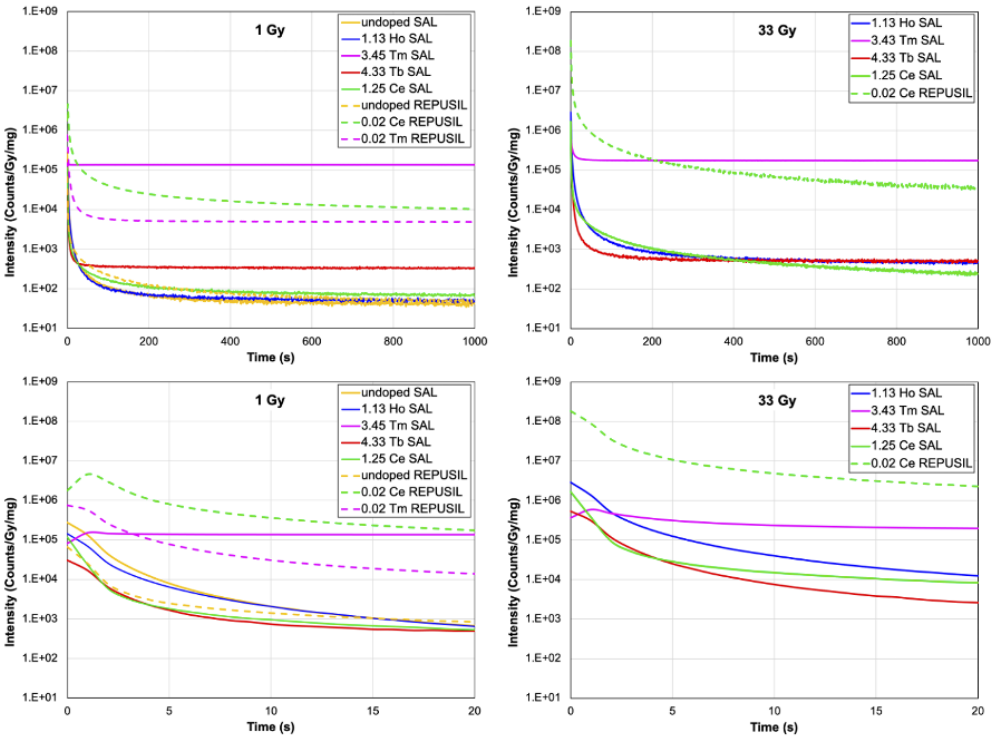

Fig. 5. OSL decay curves for different RE dopants measured using stimulation at 470 nm and a Hoya U340 filter for detection in the 250-400 nm wavelength region at 1 Gy dose (left) and 33 Gy dose (right) over whole measured time frame of 1000 s (top) and over first 20 s (bottom).

The Tm SAL and Tm REPUSIL samples exhibit background levels with high OSL counts. This phenomenon is particularly pronounced for the Tm SAL sample, where essentially no bleaching is observed. The Ce REPUSIL sample shows a similar decay behavior as the Ce SAL sample but with ~100 × higher OSL counts. These differences in OSL decay behavior are attributed to different recombination center types, RE concentration quenching and upconversion fluorescence as follows.

Optical Materials EXPRESS

The occurrence of OSL for the undoped SAL sample is surprising, considering the absence of RL and TL for this sample. The similarity of the OSL decay behavior for undoped SAL and REPUSIL samples indicates that both glass samples have the same OSL mechanism. To explain the occurrence of OSL in the undoped samples, we propose the hypothesis that the OSL is caused by radiation-induced defects (RIDs) that act as intrinsic recombination centers with luminescence in the OSL detection range. A potential RID is the oxygen deficient center, ODC(II), which was formed via neutron or laser irradiation in silica glass [43,44] and exhibits fluorescence at 280 nm in the OSL detection range of 250-400 nm. The absence of RL and TL indicates that the OSL was excited via electrons in deep traps through optical stimulation. Likely candidates for such deep electron traps, releasing the trapped electrons via 470 nm light but not via heat stimulation, are the intrinsic defect centers that are formed during glass fabrication and show PL at 520 nm before irradiation. PL measurements in the UV will be used in the future to confirm the formation of UV-fluorescent RID centers in SAL and REPUSIL glass.

The similar OSL behavior of the Ho, Ce and Tb SAL samples relative to the undoped SAL sample suggests that for these RE doped samples, the OSL is also caused by the RID center but not by RE luminescence. For the Ho samples, this hypothesis agrees with the absence of Ho^{3+} PL, RL and TL in the OSL detection range. However, for the Tb and Ce samples, this mechanism is in contrast to the presence of RE based PL, RL and TL in the OSL detection range (Section 3.2). The reasons for this discrepancy are discussed in the next section.

The ~100 × higher OSL for both 1 and 33 Gy irradiation for the weakly doped Ce REPUSIL sample compared to the highly doped Ce SAL sample correlates with ~100 × higher TL and RL for Ce REPUSIL (Fig. 5). This indicates that the Ce^{3+} ions in this glass type contribute strongly to OSL; possibly the Ce^{3+} ions act as extrinsic recombination centers with higher OSL in the detection range of 250-400 nm compared to the intrinsic recombination centers for the undoped samples and the Ce SAL sample. The absence of Ce^{3+} recombination centers (indicated by lack of Ce^{3+} based OSL) in the highly doped Ce SAL sample is attributed to concentration quenching because of the ~100 × higher Ce^{3+} concentration in the SAL sample.

The Tm SAL sample shows a peculiar behavior - a high number of OSL counts independent of time and also roughly independent of the OSL dose (200,000 ± 60,000 counts for all doses for the 2.24 and 3.45 Tm SAL samples as shown in Figure S3). Without any radiation dose, the 470 nm stimulation leads to similarly high number of luminescence counts (results not shown). This indicates that the stimulation light causes upconversion fluorescence in the OSL detection range of 250-400 nm. The time independence and higher values for the OSL counts at saturation level for the Tb SAL and Tm REPUSIL samples relative to the undoped samples as well as dose independence for the Tb SAL sample background level (Fig. S3) suggests that these samples also exhibit upconversion fluorescence. Tm^{3+} and Tb^{3+} ions are known to show upconversion fluorescence from 4f levels in the UV range (Tm: $^1I_6$ 290 nm, $^1D_2$ 360 nm; Tb: $^5G_6$ 380 nm) when excited in the visible or near-infrared [45–48]. In this work, the coincidence of the stimulation wavelength at 470 nm with the Tm^{3+} absorption band at 465 nm and the Tb^{3+} absorption band at 485 nm leads to absorption of the stimulation light by the RE ions, yielding upconversion fluorescence that is observed as time- and dose independent OSL counts at background level. The decrease of the upconversion fluorescence intensity in the order of Tm SAL > Tm REPUSIL > Tb SAL correlates with the decrease of the absorption at the stimulation wavelength of 470 nm (Fig. 1). For the Tm REPUSIL samples, the lower Tm^{3+} concentration in the REPUSIL sample causes the lower absorption. Compared to the highly doped Tm SAL sample, the lower absorption at 470 nm for the highly doped Tb sample reflects the lower absorption cross section of Tb^{3+} relative to Tm^{3+} at this wavelength. Ho^{3+} shows a high absorption at the stimulation wavelength of 470 nm but no upconversion fluorescence due to the multiphonon quenching of the Ho^{3+} fluorescence in the UV as described in Section 3.2.

Optical Materials EXPRESS

3.4. Integrated OSL intensity

The OSL counts integrated over the first 20 s (hereafter referred to as integrated OSL counts) are used for quantitative investigation of the OSL response. The Tm samples are not included due to their strong upconversion fluorescence overlapping with the OSL response as discussed above. Figure 6(a) shows the integrated OSL counts as a function of RE concentration for different dose. As there is no OSL response in the absence of beta irradiation, the data points were fitted with a line going through zero at origin (Table S3). All samples investigated show approximately linear increase of integrated OSL counts with beta irradiation dose, with the slope representing the dose sensitivity of the OSL response.

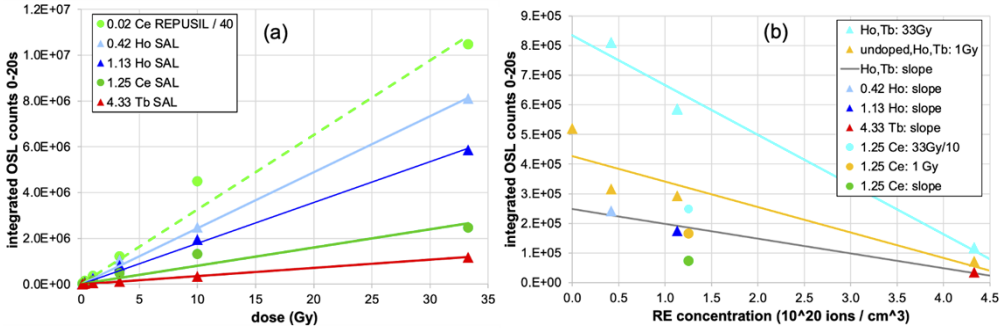

Fig. 6. OSL counts integrated over the first 20 s measured using stimulation at 470 nm and a Hoya U340 filter for detection in the 250 to 400 nm band as a function of (a) dose and (b) RE concentration. The slopes of the fitting lines shown in (a) are also plotted in (b) as a function of RE concentration using the same colors and shape for the data points.

To investigate the impact of RE concentration on the OSL of the SAL samples, we plotted the 0-20 s integrated OSL counts as a function of RE concentration for 1 Gy and 33 Gy radiation dose, as well as the slope of the OSL sensitivity lines as a function of RE concentration (Fig. 6(b), Table S3). Note that the data of the Ce REPUSIL sample are not shown as this sample shows a different OSL mechanism as explained below. The plot indicates that the OSL dose sensitivity decreases linearly with increasing RE concentration for the SAL samples with RE ions having 4f transitions in the OSL detection range (Ho^{3+}, Tb^{3+}), highlighting that the undoped sample shows highest OSL dose sensitivity. This behavior suggests that the OSL in all SAL samples is dominated by the UV-fluorescent RIDs that act as intrinsic recombination centers and are excited via electrons released from deep intrinsic traps via stimulation with 470 nm light. The RE ions do not contribute to OSL but rather hinder the OSL caused by the intrinsic RIDs. This type of OSL is hereafter referred to as intrinsic OSL. We hypothesize that the RE ions form traps or interact in such a way with the ionizing radiation that the electrons and holes are preferably trapped in shallow RE related traps and less in the deep intrinsic traps that, upon light stimulation, release the electrons interacting with the RIDs causing the OSL signal measured. Hence, the intrinsic OSL intensity connected to deep intrinsic traps and intrinsic RIDs decreases with increasing RE ion doping. The Ce SAL sample shows even lower intrinsic OSL compared to the other RE SAL samples for its respective RE concentration, which correlates with the location of the Ce^{3+} 5d energy level being furthest away from the intrinsic glass edge, which possibly enhances interferences with intrinsic defect centers.

3.5. Pulse-annealing, repeated and delayed OSL, and phosphorescence experiments

To gain insight in the thermal stability of the RID centers acting as traps and recombination centers for the OSL response, various OSL experiments were undertaken; pulse-annealing, measurement

Optical Materials EXPRESS

of OSL with a delay after irradiation, repeated OSL measurements, and phosphorescence measurement. These experiments were performed on the Tb and Ce SAL samples based on their high RL and TL prior to gaining the understanding that the OSL of the SAL samples is not directly correlated with RL and TL. The Ce REPUSIL sample is also investigated to understand the impact of RE concentration.

Pulse-annealing experiments show the temperature up to which the OSL traps and/or recombination centers are stable and not thermally drained. The pulse-annealing protocol consisted of applying a beta dose, followed by a short 470 nm stimulation pulse at 30°C as the initial measurement of OSL counts. This was followed by cycles of heating to incrementally higher temperatures (up to 450 °C), with each heating cycle followed by a short optical stimulation pulse at 30°C. The ratio of the OSL counts of these pulses to the initial OSL counts, after depletion correction, reveals the temperature range over which the OSL is thermally eroded [49].

For both the Tb and the Ce doped SAL sample, pulse-annealing revealed rapid erosion of the OSL signal intensity at increasing temperature until virtually eliminated by 175 °C (Fig. 7(a)). Such a thermal fading behavior is typical for RIDs such as the ODC(II) defect [50], which confirms the hypothesis that the OSL signal is caused by an intrinsic RID acting as luminescent recombination center via stimulation of deep traps.

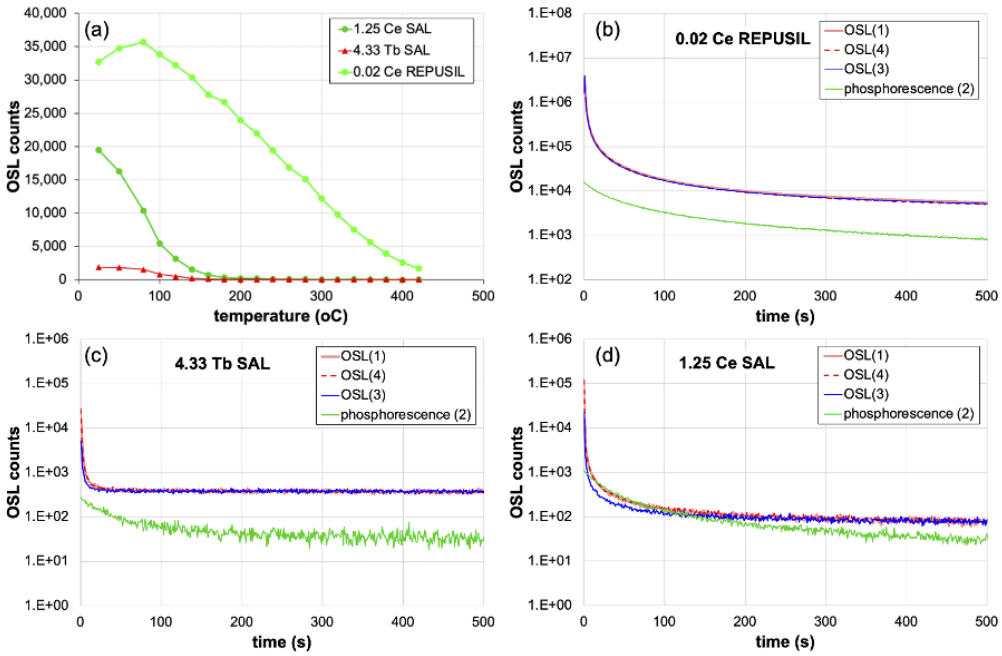

Fig. 7. (a) Pulse-annealing shown as ratio of the OSL counts per pulse to the initial OSL counts, after depletion correction, as a function of annealing temperature for Ce and Tb SAL and Ce REPUSIL samples. (b,c,d). OSL and phosphorescence measurement results for (b) 0.02 Ce REPUSIL sample, (c) 4.33 Tb SAL sample and (d) 1.25 Ce SAL sample.

The weakly doped Ce REPUSIL sample shows a different pulse-annealing behavior. First thermal transfer from shallow to deep traps is observed until ~80 °C, followed by monotonic erosion of the OSL signal until virtually eliminated by 400 °C (Fig. 7(a)). This difference in pulse-annealing behavior confirms our hypothesis that the weakly doped Ce REPUSIL sample and the highly doped Ce SAL sample exhibit different OSL recombination centers: Ce^{3+} ions in the Ce REPUSIL sample and RID centers in the Ce SAL sample.

Optical Materials EXPRESS

The sequence of OSL, phosphorescence, delayed OSL and repeated OSL measurements, each after 1 Gy irradiation, was (Fig. S4):

(1) OSL promptly after first irradiation

(2) phosphorescence promptly after second irradiation

(3) OSL measured with 17 min delay after third irradiation

(4) OSL measured promptly after fourth irradiation

The delayed OSL after the second irradiation shows the loss of stored electrons and holes via thermal decay at room temperature, which reduces the measured dose by reducing either the number of traps and/or the number of recombination centers. Repeated OSL after the fourth irradiation indicates whether an OSL measurement restores the material to its original non-irradiated state, which is important for consistent dosimeter response. Phosphorescence is a competitor effect to OSL as it causes luminescence after irradiation without light stimulation, hence phosphorescence measurement is also critical to evaluate the OSL response for practical dosimetry application.

For both the Tb and the Ce SAL sample, the OSL curves measured twice promptly and once with 17 min delay after irradiation overlap (Figs. 7(c) and (d)), indicating consistent OSL response and absence of trapped charge build-up. For the OSL measurement done with 17 min delay after irradiation, slightly lower OSL counts are observed at the beginning. This indicates that OSL is caused by a defect showing thermal fading at room temperature. This behavior is consistent with the rapid erosion of the OSL during pulse-annealing and confirms the hypothesis that the OSL is caused by intrinsic RIDs that show thermal fading.

For the Ce REPUSIL sample, the OSL curves measured twice promptly and once with 17 min delay after irradiation also overlap, but in contrast to the Ce SAL sample, the Ce REPUSIL sample does not show slightly lower OSL counts for the 17 min delayed measurement (Fig. 7(b)). This behavior correlates with higher thermal stability of the OSL during pulse-annealing (Fig. 7(a)). It confirms the hypothesis that the Ce REPUSIL and Ce SAL samples exhibit different OSL recombination centers: permanent (thermally stable) Ce^{3+} ions in Ce REPUSIL but transient RID centers that fade at room temperature in Ce SAL.

The Tb SAL sample and the Ce REPUSIL sample show negligible phosphorescence relative to OSL (less than 1% of the total counts) (Figs. 7(b) and (c)). This indicates that any untrapping of shallow traps at ambient temperature does not lead to an appreciable luminescence signal. The Ce SAL sample has ~5 times higher phosphorescence than the Tb SAL sample at the beginning, making the phosphorescence after 15 s comparable to OSL (Fig. 7(d)), which hampers practical dosimetry application.

4. Conclusions

For both the undoped SAL sample and the undoped REPUSIL sample, the OSL is dominated by intrinsic RID centers in the glass matrix itself. A likely candidate for such a defect center is the oxygen deficient center showing luminescence at 280 nm in the OSL detection range [43,44]. The luminescence from the intrinsic RID centers is stimulated via deep traps present in the glass matrix in form of permanent defect centers, possibly introduced during the glass fabrication process. A likely candidate for such a permanent defect center is the intrinsic glass defect center causing the broad PL at 520 nm, which coincides with the stimulation wavelength of 470 nm.

RE doping allows in principle the presence of additional OSL from extrinsic recombination centers due to RE luminescence. In practice, occurrence of extrinsic OSL depends on the presence and intensity of RE transitions in the OSL detection range, which is affected by radiative transition

Optical Materials EXPRESS

probability, concentration quenching and multiphonon quenching. For the OSL detection range of 250-400 nm in this study, the intensity of relevant RE transitions is affected as follows.

Multiphonon quenching plays a dominant role for the Ho^{3+} f-f luminescence transitions for high-phonon energy glasses such as SAL and REPUSIL due to small energy gaps between the 4f levels in the UV and visible range. This prevents any Ho^{3+} luminescence (PL, RL, TL) and hence any extrinsic OSL.

The absence of concentration quenching for the weakly doped Ce and Tm REPUSIL glasses provides the potential for extrinsic OSL. For the Ce REPUSIL glass, the high radiative transition probability of the spin-allowed, broad Ce^{3+} d-f luminescence at ~400 nm, whose short wavelength part is in the OSL detection range of 250-400 nm, leads to exceptionally high extrinsic OSL that is two orders of magnitude larger than the intrinsic OSL. For the Tm REPUSIL glass, the low radiative transition probability of the Tm^{3+} f-f luminescence at 360 nm in the OSL detection range leads to negligible extrinsic OSL (excluding the high upconversion background).

For the RE SAL samples, the high RE concentrations lead to concentration quenching of the RE luminescence transitions in the OSL detection range. As a result, the RE ions do not act as extrinsic recombination centers, which prevents extrinsic OSL, but the RE ions interfere with the capture of electrons and holes at the deep intrinsic traps and/or intrinsic recombination centers, leading to a decrease of the intrinsic OSL. Thus, undoped SAL is better suited for OSL measured with a photomultiplier tube at 250-400 nm detection wavelength range.

The doping of SAL and REPUSIL glasses with Tm^{3+} and Tb^{3+} ions, which exhibit an absorption close to the OSL stimulation wavelength of 470 nm and luminescent transitions in the OSL detection range, leads to upconversion fluorescence in the UV, which interferes with the OSL measurement. The intensity of the undesired upconversion fluorescence depends on the magnitude of the absorption of the stimulation light by the RE ions, which increases with increasing RE concentration and increasing absorption cross section at the stimulation wavelength. The occurrence of upconversion highlights the need for selection of a stimulation wavelength away from RE absorption.

The Tb SAL sample exhibits high luminescence at 540 nm from the $^5D_4$ level due to efficient population from the upper $^5D_3$ energy level via cross relaxation enhanced by the high Tb^{3+} concentration. The Tm samples exhibit high luminescence at 465 nm due to high radiative transition probability of this transition relative to the other Tm^{3+} luminescence transitions. Exploitation of the intense luminescence transitions of Tb^{3+} at 540 nm and Tm^{3+} at 465 nm for OSL measurement would require the use of silicon avalanche diode detectors in the range of 300-1100 nm, combined with optimization of the RE concentration to maximize the luminescence intensity.

These conclusions demonstrate that the use of RE ion doping for OSL requires matching of the OSL detection range with RE transitions that have high radiative transition probabilities and are not affected by multiphonon quenching by selecting RE transitions with large energy gap to the next lower energy level. The RE concentration needs to be optimized to control concentration quenching effects. In addition to the OSL detection wavelength range, the stimulation wavelength needs to be carefully selected, namely to be far away from RE absorption to avoid parasitic upconversion fluorescence.

The investigated SAL glass samples have the following advantages for specific OSL-based radiation sensing applications.

Of all SAL samples investigated at high irradiation dose, the Ho samples show the highest dose sensitivity, which makes them ideal as low dose fiber storage dosimeters, measuring an integrated dose response over time.

However, as the undoped sample shows higher OSL per unit dose than the Ho samples, the undoped sample shows even higher dose sensitivity. It is thus expected to be even more suited as a high dose fiber storage dosimeter.

Optical Materials EXPRESS

The undoped, and the Ho, Tb and Ce doped samples show an initial high number of OSL counts, followed by fast bleaching within ~200 s to OSL counts close to the background level. This prompt bleaching provides efficient resetting of the detector back to the pre-irradiated state.

Detailed OSL experiments for the Ce and Tb SAL samples demonstrated stable OSL sensitivity over several irradiation cycles. Phosphorescence is negligible, which prevents background build-up and false readings. In contrast to weakly doped Ce REPUSIL with RE based extrinsic recombination centers, the highly doped SAL samples show rapid erosion of the OSL signal during pulse-annealing and lower OSL counts for delayed OSL measurement due to thermal annealing of the radiation-induced intrinsic recombination centers.

These radiation response features demonstrate that the SAL samples would be unsuitable as a storage phosphor, but advantageous as a 'no false positive' detector with a short duty cycle for real-time continuous monitoring of radiation fields. Future research is necessary to determine whether undoped SAL glass with higher OSL response shows also these OSL features and negligible phosphorescence and thus would be even better suited as a 'no false positive' detector.

Funding. Australian Research Council Australian Copper-Uranium Transformation Research Hub (IH130200033); Defence Science and Technology Group; University of Adelaide; and Deutscher Akademischer Austauschdienst as part of the Australia-Germany Joint Research Corporation Scheme (Project Number: 57318923); European Regional Development Fund; European Social Fund (2011 FGR 0104, B715-11005, TNA-I-1/2010); Thüringer Ministerium für Wirtschaft, Arbeit und Technologie; Australian National Fabrication Facility (Optofab node).

Acknowledgments. This work was performed, in part, at the Optofab node of the Australian National Fabrication Facility, a company established under the National Collaborative Research Infrastructure Strategy to provide nano and micro-fabrication facilities for Australia's researchers. The authors wish to thank Donald Creighton for assistance in operating the Thermoluminescence emission spectrometer, Jan Dellith (Leibniz-IPHT) for the EPMA analysis and Kay Schuster (Heraeus Comvance) for correspondence and support regarding the manuscript.

Disclosures. The authors declare no conflicts of interest.

Data availability. Data underlying the results presented in this paper are not publicly available at this time but may be obtained from the authors upon reasonable request.

Supplemental document. See Supplement 1 for supporting content.

References

1. A. L. Huston, B. L. Justus, P. L. Falkenstein, R. W. Miller, H. Ning, and R. Altemus, "Remote optical fiber dosimetry," Nucl. Instrum. Methods in Phys. Res. B: Beam Interact. Mater. Atoms **184**(1-2), 55–67 (2001).
2. A. L. Huston, B. L. Justus, and J. L. Johnson, "Fiber-optic-coupled, laser heated thermoluminescence dosimeter for remote radiation sensing," Appl. Phys. Lett. **68**(24), 3377–3379 (1996).
3. S. O'Keeffe, D. McCarthy, P. Woulfe, M. W. D. Grattan, A. R. Hounsell, D. Sporea, L. Mihai, I. Vata, G. Leen, and E. Lewis, "A review of recent advances in optical fibre sensors for in vivo dosimetry during radiotherapy," The British J. Radiol. **88**(1050), 20140702 (2015).
4. D. D. Francesca, G. L. Vecchi, S. Girard, A. Morana, I. Reghioua, A. Alessi, C. Hoehr, T. Robin, Y. Kadi, and M. Brugger, "Qualification and calibration of single-mode phosphosilicate optical fiber for dosimetry at Cern," J. Lightwave Technol. **37**(18), 4643–4649 (2019).
5. A. Alessi, A. Guttilla, S. Girard, S. Agnello, M. Cannas, T. Robin, A. Boukenter, and Y. Ouerdane, "Radiation effects on aluminosilicate optical fibers: spectral investigations from the ultraviolet to near-infrared domains," Phys. Status Solidi A **216**(3), 1800485 (2019).
6. I. Veronese, C. De Mattia, and M. Fasoli, *et al.*, "Infrared luminescence for real time ionizing radiation detection," Appl. Phys. Lett. **105**(6), 061103 (2014).
7. E. Mones, I. Veronese, A. Vedda, G. Loi, M. Fasoli, F. Moretti, N. Chiodini, B. Cannillo, and M. Brambilla, "Ce-doped optical fibre as radioluminescent dosimeter in radiotherapy," Radiat. Meas. **43**(2-6), 888–892 (2008).
8. S. Buranurak and C. Andersen, "Fiber optically coupled radioluminescence detectors: A short review of key strengths and weaknesses of Bcf-60 and Al_2O_3:C scintillating-material based systems in radiotherapy dosimetry applications," J. Phys.: Conf. Ser. **860**, 012028 (2017).
9. N. Chiodini, A. Vedda, and I. Veronese, "Rare earth doped silica optical fibre sensors for dosimetry in medical and technical applications," Advances in Optics **2014**, 1–9 (2014).
10. J. B. Birks, "*The theory and practice of scintillation counting*," Edited by Pergamon Press, Oxford, United Kingdom, 1964.
11. S. W. S. McKeever, *Thermoluminescence of Soils*, R. W. Cahn, ed. (Cambridge University Press, 1985).
12. C. A. G. Kalnins, H. Ebendorff-Heidepriem, N. A. Spooner, and T. M. Monro, "Radiation dosimetry using optically stimulated luminescence in fluoride phosphate optical fibres," Opt. Mater. Express **2**(1), 62–70 (2012).

Optical Materials EXPRESS

13. A. S. Pradhan, J. I. Lee, and J. L. Kim, "Recent developments of optically stimulated luminescence materials and techniques for radiation dosimetry and clinical applications," J Med Phys **33**(3), 85–99 (2008).
14. N. Al Helou, H. El Hamzaoui, B. Capoen, G. Bouwmans, A. Cassez, Y. Ouerdane, M. Cannes, S. Girard, and M. Bouazaoui, "Optical responses of a copper-activated sol-gel silica glass under low-dose and low-dose rate X-ray exposures," OSA Continuum **2**(3), 563–571 (2019).
15. C. A. G. Kalnins, H. Ebendorff-Heidepriem, N. A. Spooner, and T. M. Monro, "Enhanced radiation dosimetry of fluoride phosphate glass optical fibres by terbium (III) doping," Opt. Mater. Express **6**(12), 3692–3703 (2016).
16. K. Chakrabarti, V. K. Mathur, J. F. Rhodes, and R. J. Abbundi, "Stimulated luminescence in rare-earth-doped MgS," J. Appl. Phys. **64**(3), 1363–1366 (1988).
17. S. W. S. McKeever, "Optically stimulated luminescence dosimetry," Nuclear Instruments and Methods in Physics Research Section B: Beam Interactions with Materials and Atoms **184**(1-2), 29–54 (2001).
18. R. E. Shaw, C. A. G. Kalnins, N. A. Spooner, C. Whittaker, S. Grimm, K. Schuster, D. Ottaway, J. E. Moffatt, G. Tsiminis, and H. Ebendorff-Heidepriem, "Luminescence effects in reactive powder sintered silica glasses for radiation sensing," J. Am. Ceram. Soc. **102**(1), 222–238 (2019).
19. P. Antunes, F. Domingues, M. Granada, and P. Andre, "Mechanical properties of optical fibres," in *Selected Topics on Optical Fiber Technology*, M. Yasin, ed. (Intech, 2012).
20. L. V. Nguyen, S. C. Warren-Smith, H. Ebendorff-Heidepriem, and T. M. Monro, "Interferometric high temperature sensor using suspended-core optical fibers," Opt. Express **24**(8), 8967–8977 (2016).
21. J. C. Knight, "Photonic crystal fibres," Nature **424**(6950), 847–851 (2003).
22. L. A. Benevides, A. L. Huston, B. L. Justus, P. Falkenstein, L. F. Brateman, and D. E. Hintenlang, "Characterization of a fiber-optic-coupled radioluminescent detector for application in the mammography energy range," Med. Phys. **34**(6Part1), 2220–2227 (2007).
23. M. Leich, F. Just, A. Langner, M. Such, G. Schötz, T. Eschrich, and S. Grimm, "Highly efficient Yb-doped silica fibers prepared by powder sinter technology," Opt. Lett. **36**(9), 1557–1559 (2011).
24. K. Schuster, S. Unger, C. Aichele, F. Lindner, S. Grimm, D. Litzkendorf, J. Kobelke, J. Bierlich, K. Wondraczek, and H. Bartelt, "Material and technology trends in fiber optics," Adv. Opt. Technol. **3**(4), 447–468 (2014).
25. M. F. Ando, S. Fuhrmann, Z. W. Pan, B. P. Rodrigues, T. Mori, S. G. Ebbinghaus, K. Wondraczek, S. Kitani, and L. Wondraczek, "Boson peak and structural heterogeneity in ternary SiO_2-Al_2O_3-B_2O_3 glasses," J. Am. Ceram. Soc. **104**(10), 4991–5000 (2021).
26. M. F. Ando, O. Benzine, Z. Pan, J.-L. Garden, K. Wondraczek, S. Grimm, K. Schuster, and L. Wondraczek, "Boson peak, heterogeneity and intermediate-range order in binary SiO_2-Al_2O_3 glasses," Sci. Rep. **8**(1), 5394 (2018).
27. D. Litzkendorf, S. Grimm, K. Schuster, J. Kobelke, A. Schwuchow, A. Ludwig, J. Kirchhof, M. Leich, S. Jetschke, and J. Dellith, "Study of lanthanum aluminum silicate glasses for passive and active optical fibers," Int. J. Appl. Glass Sci. **3**(4), 321–331 (2012).
28. S. Iftekhar, J. Grins, and M. Eden, "Composition–property relationships of the La_2O_3–Al_2O_3–SiO_2 glass system," J. Non-Cryst. Solids **356**(20-22), 1043–1048 (2010).
29. https://www.heraeus.com/en/hca/fused_silica_quartz_knowledge_base_1/properties_1/properties_hca.html#tabs-608478-6.
30. C. A. G. Kalnins, "Radiation effects in glasses for intrinsic optical fibre radiation dosimetry," PhD thesis. Faculty of Sciences, School of Chemistry and Physics. University of Adelaide, 2015
31. J. R. Prescott, P. J. Fox, R. A. Akber, and H. E. Jensen, "Thermoluminescence emission spectrometer," Appl. Opt. **27**(16), 3496–3502 (1988).
32. Rare Earth Doped Fiber Lasers and Amplifiers. Edited by Digonnet, MJF 2nd ed. CRC Press, 2001.
33. P. A. Tanner, C.-K. Duan, V. N. Makhov, M. Kirm, and N. M. Khaidukov, "Vacuum ultraviolet excitation spectra of lanthanide-doped hexafluoroelpasolites," J. Phys.: Condens. Matter **21**(39), 395504 (2009).
34. M. M. Shahata, "Adsorption of some heavy metal ions by used different immobilized substances on silica gel," Arabian J. Chem. **9**(6), 755–763 (2016).
35. D. Ehrt and D. Möncke, "Charge transfer absorption of Fe3+ and Fe2+ complexes and UV radiation induced defects in different glasses," in *6th ESG*. Montpellier, France, 2002.
36. J. Fournier, J. Néauport, P. Grua, E. Fargin, V. Jubera, D. Talaga, and S. Jouannigot, "Evidence of a green luminescence band related to surface flaws in high purity silica glass," Opt. Express **18**(21), 21557–21566 (2010).
37. J. M. F. van Dijk and M. F. H. Schuurmans, "On the nonradiative and radiative decay rates and a modified exponential energy gap law for 4f–4f transitions in rare earth ions," J. Chem. Phys. **78**(9), 5317–5323 (1983).
38. P. D. Dragic, M. Cavillon, and J. Ballato, "Materials for optical fiber lasers: A review," Appl. Phys. Rev. **5**(4), 041301 (2018).
39. M. Kowalska, G. Klocek, R. Piramidowicz, and M. Malinowski, "Ultra-violet emission in Ho:ZBLAN fiber," J. Alloys Compd. **380**(1-2), 156–158 (2004).
40. F. Lahoz, I. R. Mart, and J. M. Calvilla-Quintero, "Ultraviolet and white photon avalanche upconversion in Ho^{3+}-doped nanophase glass ceramics," Appl. Phys. Lett. **86**(5), 051106 (2005).
41. H. Ebendorff-Heidepriem and D. Ehrt, "Relationships between glass structure and spectroscopic properties of Eu^{3+} and Tb^{3+} doped glasses," Ber. Bunsenges. Phys. Chem. **100**(9), 1621–1624 (1996).
42. M. J. Aitken, "*Thermoluminescence dating*," Edited by GW Dimbleby, ed. Academic Press, Inc.: London, 1985.

Optical Materials EXPRESS

43. L. Skuja, "Optically active oxygen-deficiency-related centers in amorphous silicon dioxide," J. Non-Cryst. Solids **239**(1-3), 16–48 (1998).
44. J. Qian, G. Wang, D. Shen, K. Lou, Q. Fu, Z. Xia, and Q.-Z. Zhao, "Tunable point defects in hydroxyl fused silica enabled by ultrashort laser pulses: photostimulated luminescence and functional module fabrication," Opt. Mater. Express **10**(5), 1241–1248 (2020).
45. W. Tian and B. R. Reddy, "Ultraviolet upconversion in thulium-doped fluorozirconate fiber observed under two-color excitation," Opt. Lett. **26**(20), 1580–1582 (2001).
46. R. Piramidowicz, A. Bok, M. Klimczak, and M. Malinowski, "UV emission properties of thulium-doped fluorozirconate glasses," J. Lumin. **129**(12), 1874–1877 (2009).
47. L. Huang, T. Yamashita, R. Jose, Y. Arai, T. Suzuki, and Y. Ohishi, "Intense ultraviolet emission from and codoped glass ceramic containing nanocrystals," Appl. Phys. Lett. **90**(13), 131116 (2007).
48. W. J. Zhang, Q. J. Chen, Q. Qian, Q. Y. Zhang, and Z. H. Jiang, "Cooperative energy transfer in Tb^{3+}/Yb^{3+}- and $Nd^{3+}/Yb^{3+}/Tb^{3}$+-codoped oxyfluoride glasses," Physica B **405**(4), 1062–1066 (2010).
49. N. A. Spooner, B. W. Smith, O. M. Williams, D. F. Creighton, I. McCulloch, P. G. Hunter, D. G. Questiaux, and J. R. Prescott, "Analysis of luminescence from common salt (NaCl) for application to retrospective dosimetry," Radiat. Meas. **46**(12), 1856–1861 (2011).
50. S. Agnello and L. Nuccio, "Thermal stability of gamma-irradiation-induced oxygen-deficient centers in silica," Phys. Rev. B **73**(11), 115203 (2006).